

## Correlated dynamics of inclusions in a supported membrane

Naomi Oppenheimer and Haim Diamant\*

*Beverly and Raymond Sackler School of Chemistry, Tel Aviv University, Tel Aviv 69978, Israel*

(Received 1 August 2010; published 15 October 2010)

The hydrodynamic theory of heterogeneous fluid membranes is extended to the case of a membrane adjacent to a solid substrate. We derive the coupling diffusion coefficients of pairs of membrane inclusions in the limit of large separation compared to the inclusion size. Two-dimensional compressive stresses in the membrane make the coupling coefficients decay asymptotically as  $1/r^2$  with interparticle distance  $r$ . For the common case, where the distance to the substrate is of submicrometer scale, we present expressions for the coupling between distant disklike inclusions, which are valid for arbitrary inclusion size. We calculate the effect of inclusions on the response of the membrane and the associated corrections to the coupling diffusion coefficients to leading order in the concentration of inclusions. While at short distances the response is modified as if the membrane were a two-dimensional suspension, the large-distance response is not renormalized by the inclusions.

DOI: [10.1103/PhysRevE.82.041912](https://doi.org/10.1103/PhysRevE.82.041912)

PACS number(s): 87.16.D-, 87.14.ep, 47.15.gm

### I. INTRODUCTION

Biological membranes are fluid bilayers made primarily of lipid molecules [1]. From a hydrodynamic point of view such a bilayer is a quasi-two-dimensional (quasi-2D) viscous liquid, whose molecules are constrained to flow along the 2D membrane surface while exchanging momentum not only among themselves, but also with the surrounding three-dimensional (3D) solvent. Biomembranes contain also a high concentration of embedded inclusions—integral proteins and possibly also nanometer-scale domains—which perform key biological functions and are typically much larger than the lipids [1]. Thus, from the same coarse-grained perspective, a biomembrane can be viewed as a quasi-2D suspension [2]. We have recently used this perspective to investigate the correlated motion of proteins in a membrane freely floating in an unbounded liquid, and how the inclusions affect the response of such a membrane to stresses [3]. In many practical circumstances, however, the membrane is not free but attached to a solid substrate, such as the elastic scaffold of the cytoskeleton or an external surface to which a cell adheres. Additionally, in various experiments membranes are more easily studied when supported by a solid substrate. The aim of the current work, therefore, is to explore how the results of Ref. [3] are modified by the presence of such a nearby immobile surface.

Two major approaches to the hydrodynamics of free membranes have been presented. The first, by Saffman and Delbrück (SD) [4], models the membrane as a viscous liquid slab of width  $w$  and viscosity  $\eta_m/w$ , having no-slip contacts at its bounding surfaces with two semi-infinite fluids of viscosity  $\eta_f$ . The second, by Levine *et al.* [5], considers the membrane as a vanishingly thin viscoelastic film embedded in an infinite viscous fluid. The dynamics of membranes embedded in a 3D fluid have been studied also using computer simulations [6–8]. The common key feature of these theories is the fact that the membrane does not conserve momentum

in two dimensions, while the total momentum is conserved in three dimensions. Consequently, a length scale  $\kappa^{-1}$  emerges, characterizing the crossover from a 2D-like membrane response, where stresses dominantly propagate through the membrane, to a 3D-like response, where the outer fluid governs the dynamics. This length is determined by the ratio between the 2D viscosity of the membrane and the 3D viscosity of the surrounding fluid [4]. For lipid bilayers  $\kappa^{-1}$  is typically two to three orders of magnitude larger than the membrane thickness  $w$ , i.e., of micrometer scale. The work of Ref. [3] is an extension of the SD theory to cases with more than one inclusion, where there are three lengths to consider: the lateral size (radius)  $a$  of the inclusion, the SD length  $\kappa^{-1}$ , and the distance  $r$  between the inclusions. The analysis was restricted to the limit  $a \ll \min(\kappa^{-1}, r)$ , where complications related to specific details of the inclusions [9] are immaterial. We employ the same assumption in most of the current work as well.

The introduction of an immobile surface breaks the translational symmetry in the directions parallel to the membrane and, hence, qualitatively changes the hydrodynamics of the system as its total momentum is no longer conserved [2]. Models appropriate for such a scenario can be divided into two groups. The first [10–14] adopts a phenomenological approach, describing the membrane as a 2D Brinkman fluid [15], i.e., introducing a term in the 2D hydrodynamic equation for the membrane, which leaks momentum at a certain fixed rate  $\alpha^2 \nu_m$  (with  $\nu_m = \eta_m/\rho_m$  being the 2D kinematic viscosity of the membrane and  $\rho_m$  its 2D mass density). This sets a phenomenological screening length  $\alpha^{-1}$ , beyond which momentum is lost to the substrate. In the second approach [16–19] the additional length scale is explicitly determined by the thickness  $h$  of a fluid layer separating the membrane from the solid substrate. When fluid exists only between the membrane and the substrate (as in the case of a supported lipid monolayer) [16–18], or when the membrane lies at the midplane between two substrates [7,19], the large-distance effects converge to those of the phenomenological Brinkman-like approach in the limit  $h \ll \kappa^{-1}$  (i.e., for  $h$  much smaller than  $1 \mu\text{m}$ ). The momentum screening length thus

\*hdiamant@tau.ac.il; <http://www.tau.ac.il/~hdiamant>

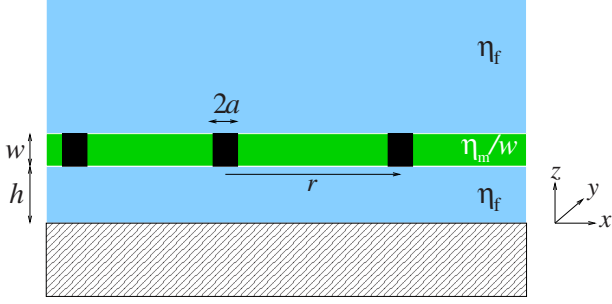


FIG. 1. (Color online) Schematic view of the model system and its parametrization.

obtained is the geometrical mean of the other two lengths,  $\alpha^{-1} \sim (\kappa^{-1}h)^{1/2}$  [17].

The current work extends the analysis of Refs. [16–18] to the realistic scenario of a supported membrane with fluid on both sides, containing more than one inclusion. In Sec. II we define the model and present the results for the hydrodynamics of a supported membrane, which will be useful for our analysis. Because of the three length scales in the model— $\kappa^{-1}$ ,  $h$ , and the interparticle distance  $r$  (assuming that  $a$  is much smaller than all three)—there are several asymptotic regimes to be considered, which are defined and discussed in Sec. II. These results are used in Sec. III to calculate the coupling diffusion coefficients of pairs of inclusions, which should be directly measurable in particle-tracking experiments. We proceed in Secs. IV and V to examine the effect of a finite concentration of inclusions on the response of the supported membrane to stresses (i.e., the effective viscosity of the membrane) and the resulting corrections to the coupling diffusion coefficients. In the practically useful limit of  $h \ll \kappa^{-1}$  we have been able to derive the large-separation coupling diffusion coefficients for inclusions of arbitrary size; these results are presented in Sec. VI. The conclusions are summarized in Sec. VII.

## II. MODEL

Our model system is similar to that of Refs. [16–18] and is schematically depicted in Fig. 1. A flat slab of viscous liquid (width  $w$  and viscosity  $\eta_m/w$ ) lies on the  $xy$  plane at a distance  $h$  away from a flat rigid surface. The space between the slab and the surface is filled with another fluid (viscosity  $\eta_f$ ). Unlike the system treated in Refs. [16–18] the space on the other side of the slab is occupied by a semi-infinite fluid of viscosity  $\eta_f$  as well. All fluids are assumed incompressible. The SD length is defined as

$$\kappa^{-1} = \frac{\eta_m}{2\eta_f}. \quad (1)$$

In the slab are rigid inclusions of radius  $a$ . Although they are depicted as cylinders, their exact shape does not affect most of our analysis; in points where it does, this will be explicitly mentioned. We do not consider effects related to curvature and thermal fluctuations of the membrane [6,20–22].

Our goal is to characterize the response of the inclusion-decorated membrane to stresses and relate it to the coupled motions of two inclusions. A common way to characterize the membrane response as a fluid medium is through the velocity Green’s function  $\mathbf{G}(\mathbf{r})$ . This tensor gives the flow velocity  $\mathbf{v}(\mathbf{r})$  of the membrane at the 2D position  $\mathbf{r}$  due to a point force  $\mathbf{F}$  exerted on the membrane at the origin in the  $xy$  plane, according to  $v_i(\mathbf{r}) = G_{ij}(\mathbf{r})F_j$  (with  $i, j = x, y$  and summation over the repeated index  $j$ ). When the separation between two inclusions is much larger than their sizes ( $r \gg a$ ), the pair mobility and pair-diffusion coefficients associated with their coupled motions can be directly obtained from the velocity Green’s function, as explained in detail in Sec. III.

In unbounded 3D liquids  $\mathbf{G}$  is the Oseen tensor [23]. We need the analogue of the Oseen tensor for the model system of Fig. 1. The velocity Green’s function for a similar model of a supported monolayer, where the upper fluid is absent, was derived in Ref. [16]. Its generalization to the case of two different fluids and two confining surfaces has been performed in Ref. [19]. We use this result while specializing to two identical outer fluids, with the upper one being semi-infinite. In Fourier space [ $\tilde{\mathbf{G}}(\mathbf{q}) = \int d^2r e^{-i\mathbf{q}\cdot\mathbf{r}} \mathbf{G}(\mathbf{r})$ ] the Green’s function is given by [19]

$$\tilde{G}_{ij}(\mathbf{q}) = \frac{1}{\eta_f q [\coth(qh) + 2q/\kappa + 1]} \left( \delta_{ij} - \frac{q_i q_j}{q^2} \right). \quad (2)$$

In the limit of an infinitely distant surface Eq. (2) coincides with the Green’s function for a free membrane [3–5],

$$\tilde{G}_{ij} \xrightarrow{h \rightarrow \infty} \tilde{G}_{ij}^f(\mathbf{q}) = \frac{1}{\eta_m q (q + \kappa)} \left( \delta_{ij} - \frac{q_i q_j}{q^2} \right). \quad (3)$$

In the other limit of a vanishingly small  $h$ , it becomes

$$\tilde{G}_{ij} \xrightarrow{h \rightarrow 0} \frac{1}{\eta_m (q^2 + \kappa q/2 + \alpha^2)} \left( \delta_{ij} - \frac{q_i q_j}{q^2} \right), \quad (4)$$

with  $\alpha = [\kappa/(2h)]^{1/2}$ . The function in Eq. (4) has two poles at  $q_{\pm} = \kappa[-1 \pm \sqrt{1 - 8/(\kappa h)}]/4$ , which in the limit  $h \rightarrow 0$  turn into  $q_{\pm} = \pm i\alpha$ . Hence, in this limit  $\tilde{\mathbf{G}}$  coincides with the 2D Brinkman-like Green’s function for an adsorbed membrane [10–14],

$$\tilde{G}_{ij} \xrightarrow{h \rightarrow 0} \tilde{G}_{ij}^a(\mathbf{q}) = \frac{1}{\eta_m (q^2 + \alpha^2)} \left( \delta_{ij} - \frac{q_i q_j}{q^2} \right). \quad (5)$$

Thus, in the strongly adsorbed limit the presence of the upper fluid merely adds a prefactor to the momentum screening length compared to the monolayer case studied earlier [17] [ $\alpha^{-1} = (2\kappa^{-1}h)^{1/2}$  instead of  $(\kappa^{-1}h)^{1/2}$ ].

The Green’s function of Eq. (2) serves as the starting point for the entire analysis to follow. It is beneficial, therefore, to begin by exploring the different asymptotic regimes that  $\mathbf{G}(\mathbf{r})$  defines. Since it depends on three lengths— $\kappa^{-1}$ ,  $h$ , and  $r$ —there are quite a few such regimes. Let us first rewrite it as a function of two length ratios,

$$G_{ij}(\mathbf{r}) = \frac{1}{\eta_f h} g_{ij}(\kappa^{-1}/h, \mathbf{r}/h),$$

$$g_{ij} = \frac{1}{(2\pi)^2} \int d^2k e^{ik \cdot (\mathbf{r}/h)} \frac{1}{k[\coth k + (2\kappa^{-1}/h)k + 1]}$$

$$\times \left( \delta_{ij} - \frac{k_i k_j}{k^2} \right), \quad (6)$$

thus making the asymptotics more transparent.

### A. Adsorbed regime: $h \ll \kappa^{-1}$

In this commonly encountered regime, where the distance to the substrate is much smaller than the SD length, the integral in Eq. (6) is governed for all values of  $r$  by small  $k$ , whereby  $\coth k + (2\kappa^{-1}/h)k \approx 1/k + (2\kappa^{-1}/h)k$ . Due to the argument presented below Eq. (4), the Green's function coincides with  $\tilde{\mathbf{G}}^a$  of Eq. (5). Inverting it to real space, one gets

$$G_{ij}^a(\mathbf{r}) = \frac{1}{2\pi\eta_m} \left[ \frac{1}{2} [K_0(\alpha r) + K_2(\alpha r)] \delta_{ij} - K_2(\alpha r) \frac{r_i r_j}{r^2} \right]$$

$$- \frac{1}{2\pi\eta_m \alpha^2 r^2} \left( \delta_{ij} - \frac{2r_i r_j}{r^2} \right), \quad (7)$$

where  $K_n$  are modified Bessel functions of the second kind. The first term in Eq. (7) is short ranged, decaying exponentially with  $\alpha r$ . It arises from shear stresses in the membrane, which get screened for  $r > \alpha^{-1}$ . The second term is long ranged, decaying only as  $1/r^2$  and originating from compressive stresses in the membrane. The effect of such stresses on the steady flow is that of an effective 2D mass dipole [2], whose magnitude is proportional to  $(\eta_m \alpha^2)^{-1} \sim h/\eta_f$ , independent of membrane viscosity.

Thus, the adsorbed regime is subdivided into two regions reflecting different physics. In the *adsorbed near* region,  $r \ll \alpha^{-1} = (2\kappa^{-1}h)^{1/2} \ll \kappa^{-1}$ , the response is governed by the yet-unscreened 2D shear stresses in the membrane. Expanding Eq. (7) in small  $\alpha r$ , we have

$$G_{ij}(\mathbf{r}) \approx G_{ij}^{\text{an}}(\mathbf{r}) = \frac{1}{4\pi\eta_m} \left\{ -[\ln(\alpha r/2) + \gamma + 1/2] \delta_{ij} + \frac{r_i r_j}{r^2} \right\}$$

$$+ O[(\alpha r)^2/\eta_m], \quad (8)$$

where  $\gamma$  is Euler's constant. This result coincides with the Oseen tensor of a momentum-conserving 2D liquid, exhibiting the well-known logarithmic behavior of this problem, with a cutoff length of  $\alpha^{-1}$ . In the *adsorbed far* region,  $r \gg \alpha^{-1} = (2\kappa^{-1}h)^{1/2} \gg h$ , the response is due to long-ranged compressive stresses, yielding

$$G_{ij}(\mathbf{r}) \approx G_{ij}^{\text{af}}(\mathbf{r}) = -\frac{h}{2\pi\eta_f r^2} \left( \delta_{ij} - \frac{2r_i r_j}{r^2} \right)$$

$$+ O[(\alpha r)^{-1/2} e^{-\alpha r}/\eta_m]. \quad (9)$$

Note that, since in the adsorbed regime  $h < \alpha^{-1} < \kappa^{-1}$ , the adsorbed near region includes distances  $r$  both smaller and larger than  $h$ , and the adsorbed far one includes distances both smaller and larger than  $\kappa^{-1}$ .

### B. Hovering regime: $\kappa^{-1} \ll h$

In this regime, where the thickness  $h$  of the fluid layer between the membrane and the substrate is the larger length scale, the asymptotes of Eq. (6) depend on the value of  $r/h$ . For  $r \ll h$  the integral in Eq. (6) is governed by large  $k$ , whereby  $\coth k + (2\kappa^{-1}/h)k \approx 1 + (2\kappa^{-1}/h)k$ . The Green's function then coincides with that of a free membrane,  $\tilde{\mathbf{G}}^f$  of Eq. (3). This is the case studied in Ref. [3]. Inverting  $\tilde{\mathbf{G}}^f$  to real space [3,5] yields

$$G_{ij}^f(\mathbf{r}) = \frac{1}{4\eta_m} \left\{ \left[ H_0(\kappa r) - \frac{H_1(\kappa r)}{\kappa r} - \frac{1}{2} [Y_0(\kappa r) - Y_2(\kappa r)] \right. \right.$$

$$+ \left. \frac{2}{\pi(\kappa r)^2} \right] \delta_{ij} - \left[ H_0(\kappa r) - \frac{2H_1(\kappa r)}{\kappa r} + Y_2(\kappa r) \right.$$

$$\left. + \frac{4}{\pi(\kappa r)^2} \right] \frac{r_i r_j}{r^2} \right\}, \quad (10)$$

where  $Y_n$  are Bessel functions of the second kind, and  $H_n$  are Struve functions.

The free behavior is subdivided into two regions having different physics. For  $r \ll \kappa^{-1} \ll h$  we have the *free near* region, where Eq. (10) becomes

$$G_{ij}(\mathbf{r}) \approx G_{ij}^{\text{fn}}(\mathbf{r}) = \frac{1}{4\pi\eta_m} \left\{ -[\ln(\kappa r/2) + \gamma + 1/2] \delta_{ij} + \frac{r_i r_j}{r^2} \right\}$$

$$+ O(\kappa r/\eta_m). \quad (11)$$

As in the adsorbed near region [Eq. (8)] the response in the free near region is governed by 2D shear stresses in the membrane. The difference is in the cutoff length, which in this case is  $\kappa^{-1}$  rather than  $\alpha^{-1}$ . In the *free far* region,  $\kappa^{-1} \ll r \ll h$ , Eq. (10) yields

$$G_{ij}(\mathbf{r}) \approx G_{ij}^{\text{ff}}(\mathbf{r}) = \frac{1}{4\pi\eta_f} \frac{r_i r_j}{r^3} + O[(\kappa r)^{-2}/\eta_m]. \quad (12)$$

Both the  $1/r$  decay and the dependence on  $\eta_f$  rather than  $\eta_m$  indicate that the response in this region is due to shear stresses in the 3D fluid on the two sides of the membrane.

In the last asymptotic region,  $\kappa^{-1} \ll h \ll r$ , although  $h$  is the larger characteristic length, the distance  $r$  is sufficiently large to make the fact that the membrane is supported rather than free come into play. In this *supported* region the integral in Eq. (6) is governed by small  $k$ ; yet, unlike the adsorbed regime,  $\coth k + (2\kappa^{-1}/h)k \approx 1/k + k/3$ , independent of  $\kappa$ . The resulting Green's function is

$$\tilde{G}_{ij}(\mathbf{q}) \approx \tilde{G}_{ij}^s(\mathbf{q}) = \frac{1}{\eta_f h (q^2/3 + q/h + h^{-2})} \left( \delta_{ij} - \frac{q_i q_j}{q^2} \right), \quad (13)$$

TABLE I. Summary of asymptotic spatial regimes and their corresponding notation.

Regime	Subregion	Definition	Spatial dependence	Mechanism
Adsorbed		$h \ll \kappa^{-1}$		
	Near	$r \ll \alpha^{-1} \equiv (2\kappa^{-1}h)^{1/2}$	$\ln(\alpha r)$	2D shear
	Far	$r \gg \alpha^{-1}$	$r^{-2}$	2D compression
Hovering		$\kappa^{-1} \ll h$		
	Free near	$r \ll \kappa^{-1}$	$\ln(\kappa r)$	2D shear
	Free far	$\kappa^{-1} \ll r \ll h$	$r^{-1}$	3D shear
	Supported	$r \gg h$	$r^{-2}$	2D compression

which has two poles, both depending on  $h$  alone—i.e.,  $h$  is the sole momentum screening length in this region. Inverting Eq. (13) to real space and taking the limit  $r \gg h$  yields

$$G_{ij}(\mathbf{r}) \approx G_{ij}^s(\mathbf{r}) = -\frac{h}{2\pi\eta_f r^2} \left( \delta_{ij} - \frac{2r_i r_j}{r^2} \right) + O[h^2/(\eta_f r^3)]. \quad (14)$$

Thus, despite differences in the details ( $\alpha^{-1}$  vs  $h$  as the length scale for momentum loss), the asymptotic responses in the adsorbed far and supported regions [Eqs. (9) and (14), respectively] turn out to be identical, both arising from 2D compressive stresses due to an effective mass dipole of magnitude  $\sim h/\eta_f$ . Note, however, that the correction to the leading mass-dipole term in Eq. (9) is exponentially small, whereas in the supported region the correction is algebraic. This reflects the fact that in the adsorbed region the upper fluid is insignificant, whereas in the supported region it does play a role, albeit not a dominant one. The various spatial regimes are summarized in Table I.

### III. CORRELATED DIFFUSION

The Green's function of Eq. (6) gives the membrane flow velocity at position  $\mathbf{r}$  in response to a unit force exerted on it at the origin. In the limit  $r \gg a$ , addressed in this paper, the same Green's function also gives the coupling mobility tensor,  $B_{12,ij}(\mathbf{r})$ —i.e., the velocity of one particle due to a unit force acting on another, where the positions of the two particles are separated by the vector  $\mathbf{r}$ ,  $v_{1,i} = B_{12,ij}(\mathbf{r})F_{2,j}$  (with summation over the repeated index  $j$ ). From the mobility tensor the coupling diffusion tensor  $D_{12,ij}(\mathbf{r})$  readily follows via the Einstein relation,  $D_{12,ij} = k_B T B_{12,ij}$ , with  $k_B T$  being the thermal energy. The  $x$  axis can be defined, without loss of generality, along the line connecting the pair,  $\mathbf{r} = r\hat{x}$ . This choice leads, by symmetry, to  $D_{12,xy} = 0$ . The coupled diffusion of the two particles is then fully characterized by two coefficients: a longitudinal coupling diffusion coefficient,  $D_L(r) = D_{12,xx}(r\hat{x})$ , and a transverse one,  $D_T(r) = D_{12,yy}(r\hat{x})$ . Thus, in summary, we have

$$D_L(r \gg a) = k_B T G_{xx}(r\hat{x}), \quad D_T(r \gg a) = k_B T G_{yy}(r\hat{x}). \quad (15)$$

The first coefficient is associated with the coupled Brownian motion of the pair along their connecting line, while the second is associated with the coupled motion perpendicular to that line,

$$\langle \Delta x_1 \Delta x_2 \rangle = 2D_L(r)t, \quad \langle \Delta y_1 \Delta y_2 \rangle = 2D_T(r)t, \quad (16)$$

where  $\Delta x_\beta$ ,  $\Delta y_\beta$  ( $\beta=1,2$ ) are the displacements of particle  $\beta$  during time  $t$ . We shall now give the expressions for these coupling diffusion coefficients in the various asymptotic regimes (cf. Table I).

#### A. Adsorbed regime: $h \ll \kappa^{-1}$

In the adsorbed regime we get from Eqs. (7) and (15) the following coupling diffusion coefficients:

$$h \ll \kappa^{-1}: \quad D_L(r) \approx \frac{k_B T}{2\pi\eta_m} \left[ -\frac{K_1(\alpha r)}{\alpha r} + \frac{1}{\alpha^2 r^2} \right],$$

$$D_T(r) \approx \frac{k_B T}{2\pi\eta_m} \left[ K_0(\alpha r) + \frac{K_1(\alpha r)}{\alpha r} - \frac{1}{\alpha^2 r^2} \right]. \quad (17)$$

This regime is subdivided into near and far regions. In the adsorbed near region Eqs. (8) and (15) yield

$$h \ll \kappa^{-1}: \quad D_{L,T}(r \ll \alpha^{-1}) \approx \frac{k_B T}{4\pi\eta_m} [-\ln(\alpha r/2) - \gamma \pm 1/2], \quad (18)$$

whereas in the adsorbed far region we obtain from Eqs. (9) and (15)

$$h \ll \kappa^{-1}: \quad D_{L,T}(r \gg \alpha^{-1}) \approx \pm \frac{k_B T h}{2\pi\eta_f r^2}. \quad (19)$$

In Eqs. (18) and (19) the upper (lower) sign corresponds to the longitudinal (transverse) coefficient. Notice how at large distances,  $r \gg \alpha^{-1}$ , the coupling diffusion coefficients both decay as  $1/r^2$ , suggesting the dominance of the aforementioned mass dipole. The momentum at such distances is lost to the solid substrate, and the coupling is mediated by 2D compressive stresses in the membrane. The dependencies of the coupling diffusion coefficients on the separation between the inclusions for the adsorbed regime are shown in Fig. 2 along with their various asymptotes.

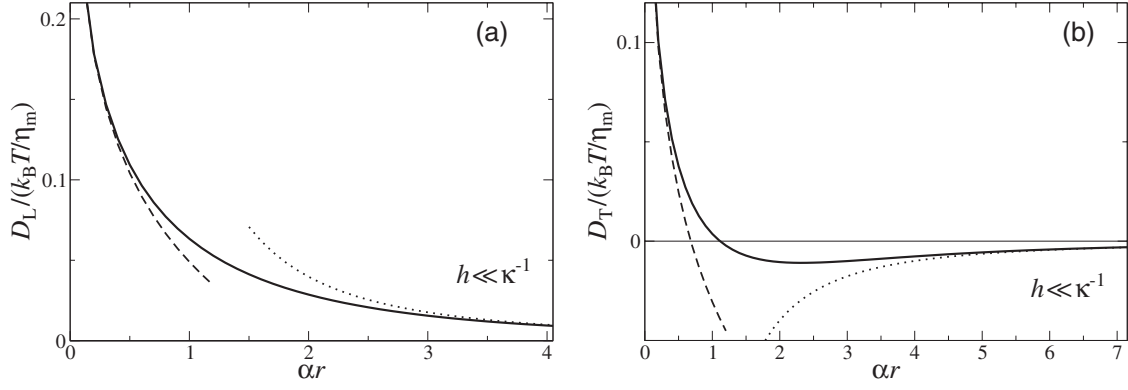


FIG. 2. (a) Longitudinal and (b) transverse coupling diffusion coefficients as functions of interparticle distance for the adsorbed regime ( $h \ll \kappa^{-1}$ ). Diffusion coefficients are scaled by  $k_B T / \eta_m$  and the distance by the momentum decay length  $\alpha^{-1}$ . The full behavior [Eq. (17), solid curve] is shown together with those in the two asymptotic regions: adsorbed near region ( $D_{L,T} \sim \ln r$ , dashed curve); adsorbed far region ( $D_{L,T} \sim \pm 1/r^2$ , dotted curve).

### B. Hovering regime: $\kappa^{-1} \ll h$

The hovering regime is divided into the free ( $r \ll h$ ) and supported ( $r \gg h$ ) behaviors. In the free limit we get from Eqs. (10) and (15)

$$\kappa^{-1} \ll h: \quad D_L(r \ll h) \approx \frac{k_B T}{4\eta_m \kappa r} \left\{ H_1(\kappa r) - Y_1(\kappa r) - \frac{2}{\pi \kappa r} \right\},$$

$$D_T(r \ll h) \approx \frac{k_B T}{4\eta_m} \left\{ H_0(\kappa r) - \frac{H_1(\kappa r)}{\kappa r} - \frac{1}{2} [Y_0(\kappa r) - Y_2(\kappa r)] + \frac{2}{\pi \kappa^2 r^2} \right\}. \quad (20)$$

This behavior is further subdivided into near and far regions. In the free near region Eqs. (11) and (15) yield the coupling diffusion coefficients as

$$\kappa^{-1} \ll h: \quad D_{L,T}(r \ll \kappa^{-1}) \approx \frac{k_B T}{4\pi\eta_m} [-\ln(\kappa r/2) - \gamma \pm 1/2], \quad (21)$$

where, again, the upper (lower) sign corresponds to the longitudinal (transverse) coefficient. Note the similarity between this result and the one in the adsorbed near region [Eq. (18)]. In both cases the coupling is governed by the behavior of the membrane as a 2D fluid, with the only difference being the cutoff of the logarithmic term. In the free far region Eqs. (12) and (15) lead to

$$\kappa^{-1} \ll h: \quad D_L(\kappa^{-1} \ll r \ll h) \approx \frac{k_B T}{2\pi\eta_m \kappa r} = \frac{k_B T}{4\pi\eta_f r},$$

$$D_T(\kappa^{-1} \ll r \ll h) \approx \frac{k_B T}{2\pi\eta_m \kappa^2 r^2} = \frac{k_B T \eta_m}{8\pi\eta_f^2 r^2}. \quad (22)$$

The coupling in this region is mediated by the outer 3D fluid, as reflected by the dependence of  $D_L$  on  $\eta_f$  and its spatial

decay as  $1/r$ . The transverse coefficient decays faster (as  $1/r^2$ ) since it arises from an effective force dipole proportional to  $\kappa^{-1} \sim \eta_m / \eta_f$  [3]. This also leads to an unusual *increasing* dependence of  $D_T$  on membrane viscosity. All of the equations in the free limit, Eqs. (20)–(22), coincide with those for a free membrane as derived in Ref. [3].

In the last region, the supported region, Eqs. (14) and (15) give the coupling diffusion coefficients

$$\kappa^{-1} \ll h: \quad D_{L,T}(r \gg h) \approx \pm \frac{k_B T h}{2\pi\eta_f r^2}, \quad (23)$$

which are identical to those in the adsorbed far region [Eq. (19)], as they arise in both cases from the same physical mechanism (2D compressive stresses in the membrane). The dependencies of the coupling diffusion coefficients on the separation between the inclusions for the hovering regime, along with the various asymptotic regions, are shown in Fig. 3.

## IV. EFFECTIVE RESPONSE

The presence of inclusions in the membrane influences its response to stresses. In regular suspensions the response far from the point of perturbation is similar to that of the particle-free liquid but with a different prefactor, depending on the volume fraction of particles,  $\phi$ . The modified prefactor defines a modified effective viscosity,  $\eta \rightarrow \eta^{\text{eff}}(\phi)$ . For a 3D suspension of hard spheres the effective viscosity, to leading order in  $\phi$ , was calculated by Einstein [24] as  $\eta^{\text{eff}} = \eta[1 + (5/2)\phi]$ . The analogous calculation for a 2D suspension of hard disks yields  $\eta^{\text{eff}} = \eta(1 + 2\phi)$  [25]. As we have seen in Sec. II, the inclusion-free supported membrane may exhibit a 2D-like response, a 3D-like one, or neither of the two. Hence, one expects a more complex modification of the response due to the presence of inclusions, depending on the various lengths in the problem. For sufficiently small distances momentum is conserved within the membrane, and we expect the response to be 2D-like. For sufficiently large distances transverse momentum is lost to the substrate, and the membrane is expected to behave neither as a 3D suspen-

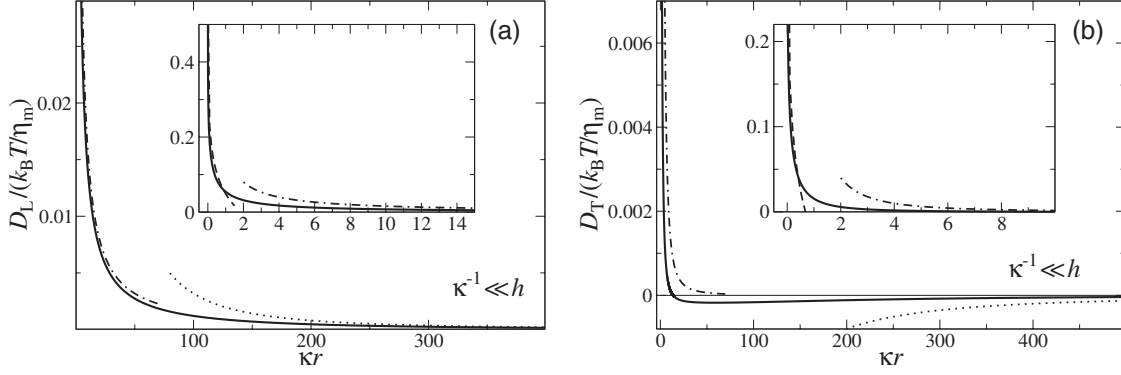


FIG. 3. (a) Longitudinal and (b) transverse coupling diffusion coefficients as functions of interparticle distance for the hovering regime ( $\kappa^{-1} \ll h$ ). Insets focus on the small-distance behavior. Diffusion coefficients are scaled by  $k_B T / \eta_m$  and the distance by the Saffman-Delbrück length  $\kappa^{-1}$ . The full behavior [numerical integration of Eq. (6) using  $\kappa h = 10^2$ , solid curve] is shown together with those in the various asymptotic regions: free near region ( $D_{L,T} \sim \ln r$ , dashed curve); free far region ( $D_L \sim 1/r$  and  $D_T \sim 1/r^2$ , dashed-dotted curve); supported region ( $D_{L,T} \sim \pm 1/r^2$ , dotted curve).

sion nor as a 2D one. Heuristically, and also based on the results for a free membrane [3], we anticipate that the effective response of the supported membrane, having an area fraction  $\phi$  of disklike inclusions,  $\mathbf{G} \rightarrow \mathbf{G}^{\text{eff}}$ , will be obtained by the following transformation of the parameters:

$$\begin{aligned} \eta_m &\rightarrow \eta_m^{\text{eff}}(\phi) \approx \eta_m(1 + 2\phi), \\ \kappa &\rightarrow \kappa^{\text{eff}}(\phi) = 2\eta_l/\eta_m^{\text{eff}} \approx \kappa(1 - 2\phi), \\ \alpha &\rightarrow \alpha^{\text{eff}}(\phi) = [\kappa^{\text{eff}}/(2h)]^{1/2} \approx \alpha(1 - \phi). \end{aligned} \quad (24)$$

We now proceed to proving that this is indeed the case.

Let us begin with an inclusion-free membrane and apply an in-plane localized force density  $\mathbf{F}\delta(\mathbf{r})$  at the origin. The resulting flow velocity field of the membrane is given by  $v_i^{(0)}(\mathbf{r}) = G_{ij}(\mathbf{r})F_j$ , where  $\mathbf{G}(\mathbf{r})$  is the Green's function discussed in Sec. II [Eq. (6)]. Next, let us consider the change in velocity at position  $\mathbf{r}$ ,  $\delta v(\mathbf{r}, \mathbf{r}')$ , due to a single disklike inclusion located at  $\mathbf{r}'$ . No force or torque is acting on the inclusion and, hence, its leading correction to the flow velocity is through the force dipole (stresslet)  $\mathbf{S}$  that it introduces,  $\delta v_i = S_{kj}(\mathbf{r}') \partial_k G_{ij}(\mathbf{r} - \mathbf{r}')$ . There is a local relation between  $\mathbf{S}(\mathbf{r}')$  and the inclusion-free velocity field at  $\mathbf{r}'$ , given by

$$S_{ij} = 2\pi\eta_m a^2 \left(1 + \frac{1}{8}a^2 \nabla^2\right) (\partial_j v_i^{(0)} + \partial_i v_j^{(0)}). \quad (25)$$

This membrane analogue of Faxén's second relation [23] was derived in Ref. [3] for a free membrane under the assumption  $\kappa a \ll 1$ . It remains valid in the current case of a supported membrane, provided that  $a \ll \min(\kappa^{-1}, \alpha^{-1})$ .

In the next stage we consider randomly distributed inclusions, occupying an area fraction  $\phi$  of the membrane. We restrict the calculation to the leading (linear) order in  $\phi$ , where static correlations as well as hydrodynamic interactions between inclusions can be neglected. The average correction to the flow velocity is given then by integration over

all possible positions  $\mathbf{r}'$  of inclusions, multiplied by the uniform probability density of finding an inclusion centered at that position,  $\phi/(\pi a^2)$ ,

$$\langle \delta v_i(\mathbf{r}) \rangle = \frac{\phi}{\pi a^2} \int d^2 r' S_{kj}(\mathbf{r}') \partial_k G_{ij}(\mathbf{r} - \mathbf{r}'). \quad (26)$$

The convolution in Eq. (26) is conveniently handled in Fourier space,

$$\begin{aligned} \langle \delta \tilde{v}_i(\mathbf{q}) \rangle &= \frac{\phi}{\pi a^2} \tilde{S}_{kj}(\mathbf{q}) i q_k \tilde{G}_{ij}(\mathbf{q}) \\ &= -2\phi \frac{2q/\kappa}{\coth(qh) + 2q/\kappa + 1} \tilde{G}_{ij}(\mathbf{q}) F_j, \end{aligned} \quad (27)$$

where in the last equation we have used Eqs. (2) and (25) while neglecting the term of order  $(qa)^2$  in Eq. (25). Writing  $\tilde{v}_i = \tilde{v}_i^{(0)} + \langle \delta \tilde{v}_i \rangle = \tilde{G}_{ij}^{\text{eff}} F_j$ , we identify the effective Green's function as

$$\tilde{\mathbf{G}}^{\text{eff}} = \left[ 1 - 2\phi \frac{2q/\kappa}{\coth(qh) + 2q/\kappa + 1} \right] \tilde{\mathbf{G}}. \quad (28)$$

It is readily verified that the same result is obtained from Eq. (2) through the transformation defined in Eq. (24) and expansion to linear order in  $\phi$ .

The  $q$  dependence of the renormalization factor in Eq. (28) reflects the aforementioned complex response of the inclusion-decorated membrane. In the  $q \rightarrow \infty$  limit the prefactor becomes  $1 - 2\phi$ , as in a 2D suspension [25]. In the opposite limit of  $q \rightarrow 0$  the prefactor tends to unity—i.e., the inclusions have no effect on the large-distance velocity response of the membrane. To analyze the effective response in more detail, away from these two limits, one may invert Eq. (28) back to real space in the desired limit. Alternatively, one can substitute the transformation defined in Eq. (24) in the various limiting expressions, already derived for  $\mathbf{G}(\mathbf{r})$  in Sec. II [Eqs. (7)–(14)], and expand those expressions to linear order in  $\phi$ . Either of these two procedures yields the effec-

tive response of the membrane in the various regimes listed in Table I. We now examine the resulting expressions for the different regimes.

In the adsorbed regime,  $h \ll \kappa^{-1}$ , the substrate affects the response of the membrane. The correction to the Green's function of Eq. (7) due to the presence of inclusions is given in this regime by

$$h \ll \kappa^{-1}: \quad \mathbf{G}^{\text{eff}} \simeq \mathbf{G}^{\text{a}} + \delta\mathbf{G}^{\text{a}},$$

$$\delta\mathbf{G}_{ij}^{\text{a}}(\mathbf{r}) = \frac{\phi}{2\pi\eta_{\text{m}}} \left[ [-K_0(\alpha r) + \alpha r K_1(\alpha r)] \delta_{ij} - \alpha r K_1(\alpha r) \frac{r_i r_j}{r^2} \right]. \quad (29)$$

In the hovering free regions,  $\kappa^{-1} \ll h$  and  $r \ll h$ , the membrane is insensitive to the presence of the substrate. The correction to the Green's function of Eq. (10) for these free regions is

$$\kappa^{-1} \ll h: \quad \mathbf{G}^{\text{eff}} \simeq \mathbf{G}^{\text{f}} + \delta\mathbf{G}^{\text{f}},$$

$$\begin{aligned} \delta\mathbf{G}_{ij}^{\text{f}}(\mathbf{r}) = \frac{\phi}{2\eta_{\text{m}}} & \left\{ \frac{1 - (\kappa r)^2}{(\kappa r)^2} \left[ \frac{2}{\pi(\kappa r + 1)} + \kappa r [H_{-1}(\kappa r) \right. \right. \\ & \left. \left. + Y_1(\kappa r)] \right] \delta_{ij} + \left[ \frac{4(\kappa r - 1)}{\pi(\kappa r)^2} + \frac{(\kappa r)^2 - 2}{\kappa r} [H_{-1}(\kappa r) \right. \right. \\ & \left. \left. + Y_1(\kappa r)] - H_0(\kappa r) + Y_0(\kappa r) \right] \frac{r_i r_j}{r^2} \right\}. \quad (30) \end{aligned}$$

These two limiting cases (adsorbed and hovering free) are further subdivided into near and far regions. The near regions of both cases are governed by 2D shear stresses, leading to an effective response similar to that of a 2D particulate liquid with a leading logarithmic behavior. The differences arise from the different cutoff lengths:  $\alpha^{-1}$  in the adsorbed near region and  $\kappa^{-1}$  in the free near region. The different dependencies of these lengths on the membrane viscosity lead to slightly different concentration corrections as  $\eta_{\text{m}}$  is modified to  $\eta_{\text{m}}^{\text{eff}}$ . In the adsorbed near region,  $r \ll \alpha^{-1} \ll \kappa^{-1}$ , the correction to the Green's function of Eq. (8) is given by

$$\begin{aligned} h \ll \kappa^{-1}, \quad r \ll \alpha^{-1}: \quad \mathbf{G}^{\text{eff}} & \simeq (1 - 2\phi) G_{ij}^{\text{an}} + \frac{\phi}{4\pi\eta_{\text{m}}} \delta_{ij} \\ & = \frac{1}{4\pi\eta_{\text{m}}} \left\{ \left\{ - (1 - 2\phi) [\ln(\alpha r/2) \right. \right. \\ & \quad \left. \left. + \gamma + 1/2] + \phi \right\} \delta_{ij} \right. \\ & \quad \left. + (1 - 2\phi) \frac{r_i r_j}{r^2} \right\}. \quad (31) \end{aligned}$$

For the free near region,  $r \ll \kappa^{-1} \ll h$ , the Green's function of Eq. (11) is modified according to

$$\begin{aligned} r \ll \kappa^{-1} \ll h: \quad \mathbf{G}^{\text{eff}} & \simeq (1 - 2\phi) G_{ij}^{\text{fn}} + \frac{\phi}{2\pi\eta_{\text{m}}} \delta_{ij} \\ & = \frac{1}{4\pi\eta_{\text{m}}} \left\{ - (1 - 2\phi) [\ln(\kappa r/2) + \gamma \right. \\ & \quad \left. + 1/2] + 2\phi \right\} \delta_{ij} + (1 - 2\phi) \frac{r_i r_j}{r^2}. \quad (32) \end{aligned}$$

Equation (32) has already been derived in Ref. [3] for a free membrane.

For all other regions we find no modification of the dominant term in the membrane response due to the presence of inclusions. This is because the response in these regions is governed by mechanisms which are unrelated to the propagation of 2D shear stresses in the membrane and, therefore, insensitive to membrane properties. In the adsorbed far region,  $h \ll \kappa^{-1}$  and  $r \gg \alpha^{-1}$ , and the supported region,  $\kappa^{-1} \ll h \ll r$ , shear stresses are lost to the substrate. The remaining compressive effect (effective mass dipole) is insensitive to the presence of inclusions since the membrane is assumed to be incompressible. Thus, the dominant response in these regions is given by the unperturbed Eqs. (9) and (14). In the free far region,  $\kappa^{-1} \ll r \ll h$ , the response is dominated by 3D shear stresses in the adjacent fluid, which are obviously indifferent to the inclusions. Hence, in this region the dominant response remains equal to the unperturbed Eq. (12).

In the cases where the leading membrane response is not renormalized by the inclusions, there are nevertheless higher-order corrections which do depend on  $\phi$ . To conclude this section we address these large-distance corrections. In the adsorbed far region the correction to Eq. (9) is exponentially small in  $\alpha r$  and, therefore, negligible. In the free far region the leading correction to Eq. (12) is obtained from Eq. (30) in the limit  $\kappa r \gg 1$  as

$$\kappa^{-1} \ll r \ll h: \quad \mathbf{G}^{\text{eff}} \simeq \mathbf{G}^{\text{ff}} + \delta\mathbf{G}^{\text{ff}},$$

$$\delta\mathbf{G}_{ij}^{\text{ff}}(\mathbf{r}) = \frac{\phi}{\pi\eta_{\text{m}}(\kappa r)^2} \left( \delta_{ij} - \frac{2r_i r_j}{r^2} \right). \quad (33)$$

Thus, the correction is of higher order [ $1/r^2$  compared to  $1/r$  in Eq. (12)] but still long ranged. In the supported region we substitute in Eq. (28) the expansion  $\coth(qh) + 2q/\kappa \simeq (qh)^{-1} + 3qh$  and invert back to real space while assuming the limit  $r \gg h$ . This procedure yields the following correction to Eq. (14):

$$r \gg h \gg \kappa^{-1}: \quad \mathbf{G}^{\text{eff}} \simeq \mathbf{G}^{\text{s}} + \delta\mathbf{G}^{\text{s}},$$

$$\delta\mathbf{G}_{ij}^{\text{s}}(\mathbf{r}) = \frac{12\phi h^3}{\pi\eta_{\text{f}}\kappa r^5} \left( 4\delta_{ij} - \frac{5r_i r_j}{r^2} \right), \quad (34)$$

which decays algebraically but much faster than the unperturbed response ( $1/r^5$  vs  $1/r^2$ ).

## V. CORRECTED PAIR-DIFFUSION COEFFICIENTS

Substituting in Eq. (15) the effective response functions, calculated in Sec. IV, readily gives the corrections to the

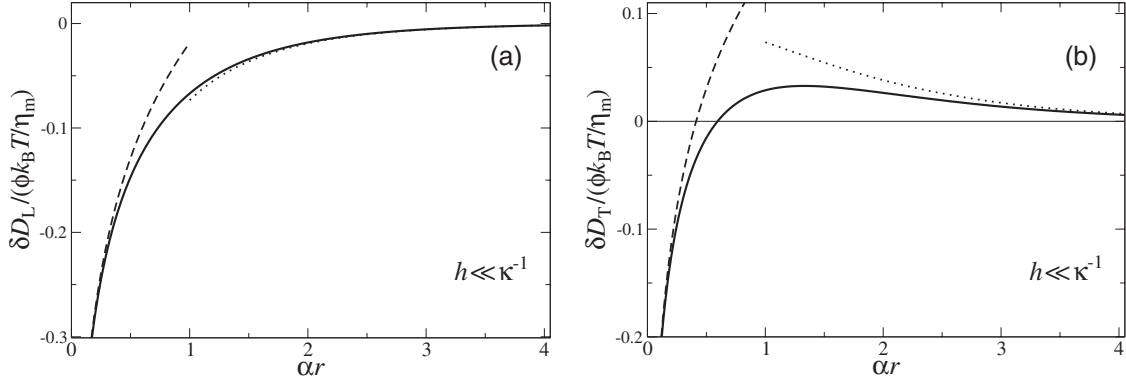


FIG. 4. Corrections to the (a) longitudinal and (b) transverse coupling diffusion coefficients as functions of interparticle distance for the adsorbed regime ( $h \ll \kappa^{-1}$ ). The corrections are scaled by  $\phi k_B T / \eta_m$  and the distance by the momentum-screening length  $\alpha^{-1}$ . The full behavior [Eq. (36), solid curve] is shown together with those in the two asymptotic regions: adsorbed near region [ $\delta D_{L,T} \sim \ln r$ , dashed curve]; adsorbed far region [ $\delta D_{L,T} \sim \mp (ar)^{\mp 1/2} e^{-ar}$ , dotted curve].

coupling diffusion coefficients to leading order in the area fraction of inclusions,

$$D_{L,T}^{\text{eff}} \simeq D_{L,T} + \delta D_{L,T}, \quad (35)$$

where  $D_{L,T}$  are the inclusion-free coefficients derived in Sec. III. We now provide the resulting expressions for  $\delta D_{L,T}$  in the various spatial regimes.

#### A. Adsorbed regime: $h \ll \kappa^{-1}$

In the adsorbed regime we use  $\delta G^a$  of Eq. (29) in Eq. (15) to get

$$h \ll \kappa^{-1}: \quad \delta D_L(r) \simeq -\phi \frac{k_B T}{2\pi\eta_m} K_0(ar),$$

$$\delta D_T(r) \simeq -\phi \frac{k_B T}{2\pi\eta_m} [K_0(ar) - arK_1(ar)]. \quad (36)$$

These expressions are the corrections to the bare coefficients given in Eq. (17). In the adsorbed near region they reduce to

$$h \ll \kappa^{-1}: \quad \delta D_{L,T}(r \ll \alpha^{-1}) \simeq \phi \frac{k_B T}{2\pi\eta_m} [\ln(ar/2) + \gamma$$

$$+ 1/2 \mp 1/2], \quad (37)$$

where the upper (lower) sign corresponds to the longitudinal (transverse) coefficient. Equation (37) gives the correction to the bare coefficients of Eq. (18). In the adsorbed far region,  $r \gg \alpha^{-1}$ , the corrections are exponentially small. More specifically,  $\delta D_L \sim (ar)^{-1/2} e^{-ar}$  and  $\delta D_T \sim (ar)^{1/2} e^{-ar}$ .

The behavior of the concentration corrections as a function of separation in the adsorbed regime is shown in Fig. 4. Notice the range of positive correction to  $D_T$ , i.e., the unusual increase in the transverse coupling due to the presence of inclusions.

#### B. Hovering regime: $\kappa^{-1} \ll h$

In the hovering free regions,  $\kappa^{-1} \ll h$  and  $r \ll h$ , we substitute  $\delta G^f$  of Eq. (30) in Eq. (15) to obtain

$$\kappa^{-1} \ll h: \quad \delta D_L(r \ll h) \simeq -\phi \frac{k_B T}{2\eta_m} \left[ \frac{2}{\pi(\kappa r)^2} + H_0(\kappa r) \right. \\ \left. - \frac{H_1(\kappa r)}{\kappa r} + \frac{1}{2} [Y_2(\kappa r) - Y_0(\kappa r)] \right],$$

$$\delta D_T(r \ll h) \simeq \phi \frac{k_B T}{2\eta_m} \frac{[1 - (\kappa r)^2]}{\kappa r} \left[ \frac{2}{\pi\kappa r(1 + \kappa r)} + H_{-1}(\kappa r) \right. \\ \left. + Y_1(\kappa r) \right], \quad (38)$$

which are the corrections to the coefficients of Eq. (20). The hovering free behavior is further subdivided into near and far regions. In the free near region, the expressions in Eq. (38) become

$$\kappa^{-1} \ll h: \quad \delta D_{L,T}(r \ll \kappa^{-1}) \\ \simeq \phi \frac{k_B T}{2\pi\eta_m} [\ln(\kappa r/2) + \gamma + 1 \mp 1/2], \quad (39)$$

which corrects Eq. (21). In the free far region Eq. (38) reduces to

$$\kappa^{-1} \ll h: \quad \delta D_{L,T}(\kappa^{-1} \ll r \ll h) \simeq \mp \phi \frac{k_B T}{\pi\eta_m} \frac{1}{\kappa^2 r^2}, \quad (40)$$

which are the corrections to  $D_L$  and  $D_T$  of Eq. (22). Note that in the free far region  $D_T$  and  $\delta D_T$  both decay as  $1/r^2$ , whereas  $D_L$  has a slower decay ( $\sim 1/r$ ) than its correction ( $\sim 1/r^2$ ). Thus, the longitudinal coefficient in the free far region remains essentially unaffected by the inclusions. The results for the hovering free region coincide with those derived in Ref. [3] for a free membrane.

In the last region, the supported region, where  $r \gg h \gg \kappa^{-1}$ , the dominant term in the large-distance response [Eq. (14)] is insensitive to the properties of the membrane. The corrections to the coupling diffusion coefficients of Eq. (23), therefore, are of higher order. Substituting  $\delta G^s$  of Eq. (34) in Eq. (15), we get

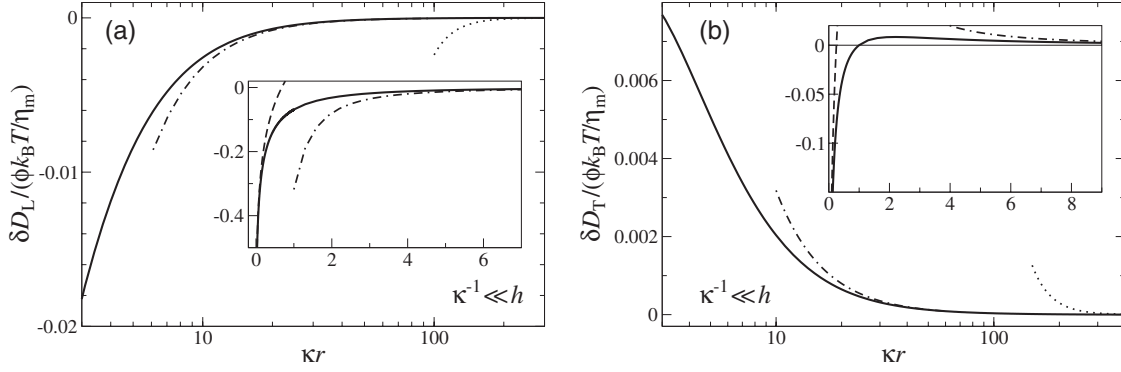


FIG. 5. Corrections to the (a) longitudinal and (b) transverse coupling diffusion coefficients as functions of interparticle distance for the hovering regime ( $\kappa^{-1} \ll h$ ). Insets focus on the small-distance behavior. Corrections are scaled by  $\phi k_B T / \eta_m$  and the distance by the Saffman-Delbrück length  $\kappa^{-1}$ . The full behavior [numerical inversion of Eq. (28) using  $\kappa h = 10^2$ , solid curve] is shown together with the asymptotes for the free near region ( $\delta D_{L,T} \sim \ln r$ , dashed curve) and free far region ( $\delta D_{L,T} \sim \mp 1/r^2$ , dashed-dotted curve). At much larger distances the supported region ( $\delta D_{L,T} \sim \mp 1/r^5$ , dotted curve) sets in.

$$\begin{aligned} \kappa^{-1} \ll h: \quad \delta D_L(r \gg h) &\approx -\phi \frac{12k_B T h^3}{\pi \eta_f \kappa r^5}, \\ \delta D_T(r \gg h) &\approx \phi \frac{48k_B T h^3}{\pi \eta_f \kappa r^5}. \end{aligned} \quad (41)$$

The spatial behavior of the concentration corrections as a function of separation in the hovering regime is shown in Fig. 5. Notice again the broad range of positive correction to  $D_T$ , where the transverse coupling increases with the concentration of inclusions. This is a consequence of the unusual dependence of the bare coefficient on membrane viscosity. [See Eq. (22) and the text below it.]

## VI. CORRELATED DIFFUSION OF LARGE INCLUSIONS

The entire analysis so far has relied on the assumption that the inclusion size is much smaller than any other length in the system,  $a \ll \min(\kappa^{-1}, h, r)$ . Consequently, the coupling diffusion coefficients derived in Sec. III were independent of the size and shape of the inclusions. In the adsorbed far region ( $r \gg \alpha^{-1} \gg h$ ) we can depart from this assumption and derive the large-separation coupling diffusion coefficients for large disklike inclusions. In principle, the calculation of pair mobilities for two large particles is technically hard—one needs to solve the flow equations with boundary conditions on the surfaces of the two particles as they move with prescribed velocities (or under prescribed forces). For the adsorbed far region, however, there is a scheme that bypasses this difficulty altogether. It is based on symmetry considerations and the knowledge of the exact flow field away from a single moving disk.

In the adsorbed regime our model becomes equivalent to an effective 2D Brinkman fluid [15]—i.e., an incompressible fluid with momentum decay—as previously studied in Refs. [10–13]. This is clearly seen in the corresponding velocity response function [Eq. (5)], which contains a momentum decay length  $\alpha^{-1}$ .

First, let us recall—for the adsorbed regime—the far flow in the membrane due to a point force  $\mathbf{F}$ . According to Eq. (9)

this flow is the same as the one emanating from an effective 2D mass dipole of strength  $(h/\eta_f)\mathbf{F}$ . Now consider the flow due to a force  $\mathbf{F}$  applied to an isolated disk of radius  $a_1$ , positioned at the origin. This problem was solved for a 2D Brinkman fluid in Ref. [11]. Applying the result to our case, we get in the far field [ $r \gg \max(a_1, \alpha^{-1})$ ] the following dipolar flow:

$$\begin{aligned} v_i(\mathbf{r}) &= -\frac{h}{\eta_f} \frac{m(\alpha a_1)}{2\pi r^2} \left( \delta_{ij} - \frac{2r_i r_j}{r^2} \right) F_j, \\ m(x) &= 2 \frac{xK_0(x) + 2K_1(x)}{xK_0(x) + 4K_1(x)}. \end{aligned} \quad (42)$$

Thus, no matter how large the disk may be, the far flow remains equivalent to that induced by a 2D mass dipole; the only dependence on the particle size is through the dimensionless prefactor  $m(\alpha a)$ .

In the next step we identify the tensor multiplying  $\mathbf{F}$  in Eq. (42) with the coupling mobility of two different particles—one of radius  $a_1$  at the origin and another of vanishing radius,  $a_2 \rightarrow 0$ , at  $\mathbf{r}$ . Due to the symmetry of the coupling mobility, the same tensor also gives the velocity of a disk of radius  $a_1$ , positioned at  $\mathbf{r}$ , due to a point force  $\mathbf{F}$  applied to the membrane at the origin. Yet, the latter is the velocity acquired by a particle of radius  $a_1$  as it is embedded in a flow caused by a mass dipole of strength  $(h/\eta_f)\mathbf{F}$ . All we need to do now to get the velocity of a disk of radius  $a_1$  due to a force  $\mathbf{F}$  exerted on a sufficiently distant disk of radius  $a_2$  is to increase the mass-dipole strength at the origin from  $(h/\eta_f)\mathbf{F}$  up to  $(h/\eta_f)m(\alpha a_2)\mathbf{F}$ , the effective mass dipole created by  $\mathbf{F}$  when it is applied to a particle of radius  $a_2$ . Hence, the large-distance coupling mobility is given by

$$B_{12,ij}(\mathbf{r}) = -\frac{h}{\eta_f} \frac{m(\alpha a_1)m(\alpha a_2)}{2\pi r^2} \left( \delta_{ij} - \frac{2r_i r_j}{r^2} \right). \quad (43)$$

As explained in Sec. III, the coupling diffusion coefficients can be readily obtained from Eq. (43) as  $D_L(r) = k_B T B_{12,xx}(r\hat{x})$  and  $D_T(r) = k_B T B_{12,yy}(r\hat{x})$ , yielding

$$r \gg \max(\alpha^{-1}, a_1, a_2): \quad D_{L,T}(r) \approx \pm \frac{k_B T m(\alpha_1) m(\alpha_2) h}{2\pi\eta_f r^2}, \quad (44)$$

where the plus (minus) sign corresponds to the longitudinal (transverse) coefficient, and  $m(x)$  is defined in Eq. (42). Equation (44) gives the large-distance coupling diffusion coefficients in the adsorbed regime for two disklike inclusions of arbitrary radii.

In the limit of small inclusions,  $\alpha\alpha_\beta \ll 1$  ( $\beta=1,2$ ), we have  $m(\alpha\alpha_\beta) \approx 1$ , and the result of Sec. III [Eq. (23)] is recovered. In the opposite limit of large inclusions,  $m(\alpha\alpha_\beta) \approx 2$ ; and, therefore,

$$r \gg a_\beta \gg \alpha^{-1}: \quad D_{L,T}(r) \approx \pm \frac{2k_B T h}{\pi\eta_f r^2}. \quad (45)$$

Thus, going from small to large inclusions changes the large-distance coupling coefficients by a mere factor of 4. Interestingly, the results for very large inclusions are again independent of particle size and shape. We return to this surprising finding in the next section.

## VII. CONCLUSIONS

The aim of this work has been to characterize supported membranes as effective heterogeneous fluids. The existence of several length scales in the problem leads to various regimes that are governed by different physical mechanisms and exhibit different effective dimensionalities (either 2D or 3D); see Table I. We have provided predictions for the coupling diffusion coefficients of inclusion pairs in those various regimes, as well as their leading dependence on the concentration of inclusions in the membrane. These predictions can be directly checked in two-point microrheology experiments using Eq. (16).

Since the SD length  $\kappa^{-1}$  is typically of micrometer scale, common supported membranes should belong in the adsorbed regime,  $h \ll \kappa^{-1}$ , which is treated in Secs. III A and V A. Moreover, the limit of small inclusion size, assumed in those sections, should be generally valid since the requirement is that  $a$  be much smaller than  $\alpha^{-1} \sim (\kappa^{-1}h)^{1/2}$  rather than the stricter condition  $a \ll h$ . Hence, we expect this limit to hold for common membrane inclusions even in cases where the distance to the substrate is on the order of the inclusion size (say, a few nm only). In this common scenario of  $a \ll \alpha^{-1} \ll \kappa^{-1}$  the substrate is predicted to strongly suppress the large-distance correlations as compared to a free membrane. Comparing the results of Sec. III A with those of Ref. [3] (or with the equivalent results for the free far region in Sec. III B), we find suppression of the longitudinal and transverse coefficients by factors of orders  $h/r$  and  $\kappa h$ , respectively. Nonetheless, the correlations always remain long ranged, with their fastest possible decay being  $1/r^2$ .

For nanometer-scale separation between membrane and substrate, which is comparable to the membrane thickness, the substrate may affect the membrane properties. As long as the membrane remains fluid, such interactions are expected to merely modify the effective membrane viscosity, and the

theory presented here should remain valid. A more serious concern is the possible breakdown of the bilayer description as a uniform slab, which is inherent in the Saffman-Delbrück model and the current work. At sufficient proximity to the surface the dynamics of the two membrane leaflets might decouple. This will occur when the friction between the lower leaflet and the solid surface exceeds the one between the two leaflets. The characteristic coefficients for these two competing drags are, respectively,  $\eta_f/h \sim 10^6$  N s/m<sup>3</sup> (for  $h \sim 1$  nm) and  $10^8$  N s/m<sup>3</sup> [26]. Thus, for all relevant separations  $h$ , relative motion of the leaflets should not play a significant role, and the bilayer can be considered as a single fluid medium.

There may be cases where the inclusion size is comparable to or larger than  $\alpha^{-1}$ —for example, when the inclusion is a colloid particle or a membrane domain. We have presented expressions for the large-distance coupling coefficients in this case as well (Sec. VI). These results have been derived for the specific case of disklike inclusions, yet in both limits of small and large  $\alpha a$  they become independent of the size and shape of the inclusions. The origin of this surprising universality is that, in the adsorbed regime, the membrane responds to any size and shape of perturbation sufficiently far away, as if the perturbation were a mass dipole. The “effective inclusion”—i.e., the region around the perturbation whose dynamics determines the strength of that mass dipole—is limited in both cases of very small and very large  $a$  by the momentum decay length  $\alpha^{-1}$ .

Concerning the effective response of the supported membrane as a function of the area fraction of inclusions, we have found that the membrane viscosity is modified according to the law for 2D suspensions [25],  $\eta_m^{\text{eff}} = \eta_m(1+2\phi)$ , yet this modification should be included also in the parameters  $\kappa$  and  $\alpha$  [Eq. (24)]. The combined effect is that there is *no* renormalization of the large-distance membrane response with increasing  $\phi$ . The underlying physics is that transverse momentum is not transferred through the membrane over large distances and, hence, the response is insensitive to changes in the membrane viscosity. This insensitivity holds already for distances much smaller than the largest length scale in the problem at hand. For the common adsorbed regime,  $h \ll \kappa^{-1}$ , it is valid for  $r \gg \alpha^{-1}$ , as momentum is first lost to the substrate. For the hovering regime,  $\kappa^{-1} \ll h$ , the dependence on  $\phi$  disappears for  $r \gg \kappa^{-1}$ , as the propagation of stresses becomes dominated by the outer fluid.

The subtle effect of increasing the area fraction of inclusions on the membrane viscosity and the governing length scales influences also the corrections to the coupling diffusion coefficients (Sec. V). At sufficiently short distances the leading logarithmic terms are corrected as if the membrane were a 2D suspension, yet at large distances all corrections to the coupling coefficients vanish.

The validity of the theory presented here is limited in several important respects. Our results concerning the coupling diffusion coefficients are all valid only for large separations,  $r \gg a$ . In addition, the coupling coefficients derived in Sec. VI for large inclusions apply only in the adsorbed far region,  $r \gg \alpha^{-1} \gg h$ ; the corresponding expressions for large inclusions in the other asymptotic regions are unknown. We have restricted the analysis of the effective response and cor-

rections to the coupling coefficients to the leading linear order in the area fraction of inclusions,  $\phi$ . Deviations from the theory are expected, therefore, as  $\phi$  becomes appreciable. Nevertheless, as is clear from the discussion above, our main qualitative results—in particular, the insensitivity of the large-distance response to  $\phi$ —are expected to be valid for all values of  $\phi$ , as long as the membrane remains fluid. Finally, we have not considered membrane fluctuations, which may have a subtle interplay with the diffusion of membrane inclusions [6,22]. As membrane fluctuations are suppressed by the presence of a nearby surface [20,21], we do not expect

our main results to be significantly influenced by such effects.

#### ACKNOWLEDGMENTS

We are indebted to Shigeyuki Komura and Sanoop Ramachandran for pointing out an error in the original manuscript and for sharing their results prior to publication. We thank Matan Ben-Zion, Frank Brown, Gilad Haran, and Maria Ott for helpful discussions. This research was supported by the Israel Science Foundation (Grant No. 588/06).

- 
- [1] B. Alberts *et al.*, *Essential Cell Biology*, 2nd ed. (Garland Science, New York, 2003).
- [2] H. Diamant, *J. Phys. Soc. Jpn.* **78**, 041002 (2009).
- [3] N. Oppenheimer and H. Diamant, *Biophys. J.* **96**, 3041 (2009).
- [4] P. G. Saffman and M. Delbrück, *Proc. Natl. Acad. Sci. U.S.A.* **72**, 3111 (1975); P. G. Saffman, *J. Fluid Mech.* **73**, 593 (1976).
- [5] A. J. Levine and F. C. MacKintosh, *Phys. Rev. E* **66**, 061606 (2002); A. J. Levine, T. B. Liverpool, and F. C. MacKintosh, *Phys. Rev. Lett.* **93**, 038102 (2004); *Phys. Rev. E* **69**, 021503 (2004).
- [6] A. Naji, P. J. Atzberger, and F. L. H. Brown, *Phys. Rev. Lett.* **102**, 138102 (2009).
- [7] S. Ramachandran, S. Komura, and G. Gompper, *EPL* **89**, 56001 (2010).
- [8] B. A. Camley and F. L. H. Brown, *Phys. Rev. Lett.* **105**, 148102 (2010).
- [9] A. Naji, A. J. Levine, and P. A. Pincus, *Biophys. J.* **93**, L49 (2007).
- [10] S. Ramaswamy and G. F. Mazenko, *Phys. Rev. A* **26**, 1735 (1982).
- [11] E. Evans and E. Sackmann, *J. Fluid Mech.* **194**, 553 (1988).
- [12] Y. Y. Suzuki and T. Izuyama, *J. Phys. Soc. Jpn.* **58**, 1104 (1989).
- [13] K. Seki and S. Komura, *Phys. Rev. E* **47**, 2377 (1993); S. Komura and K. Seki, *J. Phys. II* **5**, 5 (1995); K. Seki, S. Komura and M. Imai, *J. Phys.: Condens. Matter* **19**, 072101 (2007).
- [14] Y. Tserkovnyak and D. R. Nelson, *Proc. Natl. Acad. Sci. U.S.A.* **103**, 15002 (2006).
- [15] H. C. Brinkman, *Appl. Sci. Res., Sect. A* **1**, 27 (1947).
- [16] D. K. Lubensky and R. E. Goldstein, *Phys. Fluids* **8**, 843 (1996).
- [17] H. A. Stone and A. Ajdari, *J. Fluid Mech.* **369**, 151 (1998).
- [18] T. M. Fischer, *J. Fluid Mech.* **498**, 123 (2004).
- [19] S. Ramachandran, S. Komura, K. Seki, and G. Gompper (unpublished).
- [20] S. Sankararaman, G. I. Menon, and P. B. Sunil Kumar, *Phys. Rev. E* **66**, 031914 (2002).
- [21] N. Gov, A. G. Zilman, and S. Safran, *Phys. Rev. E* **70**, 011104 (2004).
- [22] E. Reister-Gottfried, S. M. Leitenberger, and U. Seifert, *Phys. Rev. E* **81**, 031903 (2010).
- [23] W. B. Russel, D. A. Saville, and W. R. Schowalter, *Colloidal Dispersions* (Cambridge University Press, Cambridge, England, 1989).
- [24] A. Einstein, *Investigations on the Theory of the Brownian Movement* (Dover, New York, 1954).
- [25] M. Belzons, R. Blanc, J.-L. Bouillot, and C. Camoin, *C. R. Acad. Sci., Ser. B* **292**, 939 (1981).
- [26] E. Evans and A. Yeung, *Chem. Phys. Lipids* **73**, 39 (1994).